Supplement of Clim. Past, 15, 1251–1273, 2019
https://doi.org/10.5194/cp-15-1251-2019-supplement

Climate of the Past
Open Access
EGU

Supplement of

Last Millennium Reanalysis with an expanded proxy database and seasonal proxy modeling

Robert Tardif et al.

Correspondence to: Robert Tardif (rtardif@atmos.washington.edu)

S1 Introduction

This document provides supplemental information on the characteristics of newly developed statistical proxy system models (PSMs) for tree ring width proxies, and on additional verification results of the updated paleoclimate reconstructions performed within the Last Millennium Reanalysis (LMR) framework.

S2 Proxy seasonal responses

An important update to the LMR proxy modeling capabilities is the introduction of PSMs that include a representation of proxy seasonality. Two methods for defining proxy seasonality are considered: use of the seasonal response information included in the proxy metadata, and objectively determining the seasonal period that leads the best linear fit to the proxy data as part of the PSM calibration procedure. Here we examine the differences between seasonality information from these two approaches. The comparison focuses on PSMs developed for tree ring width (TRW) records as seasonality is particularly important for these proxies (Briffa et al., 2002, 2004). TRW chronologies in our proxy database originate from two distinct data sources, the PAGES 2k Consortium (2017) community-curated collection and records discussed in Breitenmoser et al. (2014), as processed by Anderson et al. (2019). The metadata describing the records in PAGES 2k Consortium (2017), including seasonality, have been established by community experts, whereas TRW seasonality annotating the Breitenmoser et al. (2014) records was defined using a simple latitude dependency (Anderson et al., 2019). Objective seasonality is described in section 2.4 of the main text.

Figure S1 shows the overall distributions of months defining seasonal temperature responses, compiled across all TRW records and centered on the annual period the proxy data describes. Distributions corresponding to metadata and objectively-derived seasonality information are shown for both TRW data sets. For tree ring records in PAGES 2k Consortium (2017), seasonality metadata information (Figure S1a) shows records are predominantly characterized by a June–August (JJA), i.e. boreal summer, response to temperature, in addition to a significant proportion of trees with an annual seasonality as indicated by the flat distribution outside of the JJA maximum. The distribution describing the Breitenmoser et al. (2014) records (Figure S1c) reflects the simple latitude-dependent approach to define seasonality. Responses are limited to JJA for northern hemispheric (NH) trees and December–February (DJF) for trees located in the southern hemisphere (SH). The small number of trees with an annual response correspond to the tropical records present in the dataset.

With seasonality information determined objectively during PSM calibration (Figs. S1b and d), a greater diversity in seasonal responses is obtained. This is most striking with the Breitenmoser et al. (2014) chronologies. Responses remain dominated by the NH summer season, however with less emphasis on annual records as evidenced by a slightly increased representation of the boreal spring and austral summer months for NH trees and SH trees respectively. We also note the greater consistency of seasonal responses to temperature

between PAGES 2k Consortium (2017) and Breitenmoser et al. (2014) TRW records.

Figure S2 presents the results with respect to temperature and precipitation seasonal responses associated with the bivariate PSMs. Distributions describing temperature seasonality are very similar to those of the univariate models shown in Fig. S1. More importantly, the distributions of the seasonal responses to precipitation shows that objectively-derived responses are significantly different than those from proxy metadata (assumed identical to temperature responses). Distributions show a number of records with sensitivity to precipitation during the nominal growing seasons (boreal summer for NH trees and austral summer for SH trees). A noteworthy feature is the maximum in the distribution shifted toward the boreal winter season in Figs. S2d and h, consistent with tree ring growth sensitivity to precipitation occurring during the cool season preceding the growth period (St. George et al., 2010; St. George, 2014). Note that the local maximum in the austral winter in Fig. S2d correspond to SH trees. As with the temperature responses, we also note the greater consistency between responses to precipitation for PAGES 2k Consortium (2017) and Breitenmoser et al. (2014) TRW records.

S3 Independent calibration-validation

Verification statistics from a series of reconstruction experiments similar to those in section 4 of the main text are presented for independent calibration and validation data during the instrumental period. Specifically, temperature reconstructions are performed using regression-based PSMs calibrated with data covering the 1920–2015 period, instead of the entire instrumental era (i.e. 1880–2015) as in the main text. To gain a perspective on reconstruction skill which is independent from calibration, verification is performed over the 40-year period of the instrumental era not considered in PSM calibration (i.e. 1880–1919). As in experiments reported in section 4.1 of the paper, only proxies from the PAGES 2k Consortium (2017) data set are assimilated.

A summary of verification skill metrics is shown in Fig. S3. We first look at the trend in the global mean temperature (GMT) characterizing the 40-yr verification period. The GMT trend during the validation period in the instrumental analyses (i.e. GISTEMP, Berkeley Earth, HadCRUT4 and MLOST), is itself found to have a large uncertainty. Values among all products range from slightly positive to about -0.35 K per 100 years (see the gray shading in Fig. S3). Despite this uncertainty, instrumental era observations indicate a cooling trend characterizing the verification period, with a consensus (average of all products) value of -0.2 K per 100 years. Comparing trends in reconstructions generated using the various PSM configurations, we see that all reconstructions are characterized by global cooling, with the trend underestimated with the univariate annual PSMs, and generally overestimated with the seasonal univariate models. The best agreement with the consensus trend is obtained when bilinear seasonal PSMs are used, along with objectively-derived proxy seasonal responses for tree-ring-width proxies. We wish to underline here LMR's ability to recover the GMT cooling during the 1880-1919 period, distinct from the 1920–2015 PSM calibration period, which is characterized by a warming trend. This result supports the fact that reconstructions with

LMR are not directly tied to, or limited by, the climate states and their evolution represented in the calibration data set, especially since the inputs to these PSMs come from climate model priors from a different time period.

With respect to the other metrics considered in evaluating the reconstructed detrended GMT and spatial temperature patterns, the skill over the 40-year verification period is generally less than the entire instrumental era (reported in the main text). A comparison of verification statistics from the 1880–1919 and 1880–2000 periods from the same series of experiments (using PSM calibrated over the complete instrumental-era data) (not shown) confirm that the decrease in skill is a characteristic of the shorter calibration period rather than related to PSMs calibrated over a particular subset of the available calibration data.

Comparing verification metrics for different PSM configurations, skill in the detrended GMT is maximized for PSMs formulated with seasonal responses from proxy metadata, particularly when tree ring width proxies are modeled with a bilinear formulation on temperature and moisture. The skill from PSMs based on objectively-derived seasonal responses are generally lower, but remains similar to results obtained with other PSMs. Skill in the representation of spatial patterns, as summarized with the global mean of the CE values calculated at every reanalysis grid points, is less skillful in reconstructions using annual univariate PSMs. The most skillful reconstruction, as indicated by the least negative mean of the gridded CE, is obtained with seasonal objective PSMs, with a bilinear formulation to model tree ring width proxies.

The independent calibration–validation results reported here are therefore generally consistent with the findings presented in the main text. In particular, the least accurate reconstructions are obtained with univariate annual PSMs, whereas reconstructions using seasonal PSMs with objectively-derived seasonal responses, along with a bivariate temperature and moisture formulation for tree ring width proxies, are found to be more skillful. Contrasts in skill are notable for GMT trends and the representation of temperature spatial patterns. Therefore, despite the decrease in the robustness of statistics inherent to verification performed over a shorter time period, the independent calibration–validation experiments support the selection of the PSM configuration reported in section 3 of the main text.

S4 Moisture variable in tree-ring-width PSMs

In the modeling of moisture-sensitive tree-ring width chronologies, soil moisture is recognized as the preferred response variable. However, a regression-based approach to proxy modeling relies on the availability of a calibration dataset. The absence, to our knowledge, of a reliable century-long soil moisture dataset is therefore an important limiting factor. The more traditional approach consists of using Palmer Severity Drought Index (PDSI) data instead of soil moisture (e.g. Steiger et al., 2018). Here we use the Dai et al. (2004) PDSI dataset to calibrate univariate "temperature or moisture" ("TorM") PSMs, instead of precipitation data from the GPCC (Schneider et al., 2014) dataset as in reconstructions discussed in the main text. With univariate "TorM" PSMs, decisions are made whether each tree-ring record is moisture sensitive or temperature sensitive by comparing moisture calibrations (with PDSI

or precipitation) and temperature calibrations (using GISTEMP calibration). The regression providing the better fit to proxy data is used to forward model the proxy record. A reconstruction using PDSI-calibrated PSMs to model the tree-rint width proxies is compared to a reconstruction using "TorM" PSMs calibrated on precipitation (results presented in the main text). All proxies other than tree-ring widths are modeled with univariate temperature PSMs. All other reconstruction parameters are the same as experiments described in the main text (100 ensemble members, CCSM4 as the prior model, 51 Monte-Carlo realizations with 75% of proxies assimilated). Covariance localization is not applied in the compared experiments.

Temperature reconstructions from both experiments are verified against instrumental-era analyses and against independent (withheld from assimilation) proxies. Results are compared in Tables S1 and S2. Verification results for the reconstruction using bivariate PSMs calibrated on temperature and precipitation, already described in main text, are included for comparison. The reconstruction skill obtained over the instrumental-era with the univariate PSMs are similar, whether PDSI or precipitation data are used for calibration. In comparison, the skill scores obtained with bivariate PSMs are more clearly superior to the univariate PSMs, particularly with the sensitive CE metric. Proxy-based verification results (Table S2) do not distinguish well between experiments, likely due to the noisy nature of the proxies used in the verification reference. Nonetheless, the balance of evidence is that bivariate temperature/precipitation PSMs are superior to the univariate "TorM" models, even when the latter are calibrated using PDSI.

S5 Covariance localization function

Spatial covariance localization is applied to manage sampling error in the LMR paleoclimate ensemble data assimilation system. It is applied to minimize the adverse impact of spurious covariances at large distances from a proxy location, which results from sample error in finite ensembles. We use the Gaspari-Cohn (Gaspari and Cohn, 1999) fifth-order polynomial with a specified cut-off radius for the localization function. Localization is applied to ensemble covariances through the w_{loc} terms shown in Eqs. 4 in the main text. To illustrate how the localization function modulates the ensemble covariances as a function of distance, we show the w_{loc} weights calculated with two localization radii (5000 and 25000 km) for a proxy site located in the Sierra Nevada mountains in California, United States (cf. Fig. S4). For the shortest localization radius considered in the paper (5000 km), we see that the assimilation of observations from this proxy site will at most influence other analysis gridpoints in North America and the easternmost part of the midlatitude Pacific Ocean. However, most of the influence is limited to western United States , as the w_{loc} is small at distances characterizing regions such as the eastern United States and Alaska for example. For a cut-off localization radius of 25000 km, the value used in the updated LMR, assimilated proxies may contribute in the updated of state elements at points across the globe as the w_{loc} weights do not decrease to zero in this case. However this influence is minimal for far away regions (ex. Indian Ocean may only be slightly influenced by the Sierra Nevada proxy). With this localization length

scale, largest proxy influence is confined to distances roughly correspondnig to continental scales.

References

Anderson, D. M., Tardif, R., Horlick, K., Erb, M. P., Hakim, G. J., Emile-Geay, J., Noone, D., Perkins, W. A., and Steig, E. J.: Additions to the Last Millennium Reanalysis multiproxy database, Data Science Journal, 18, https://doi.org/10.5334/dsj-2019-002, 2019.

Breitenmoser, P., Brönnimann, S., and Frank, D.: Forward modelling of tree-ring width and comparison with a global network of tree-ring chronologies, Clim. Past, 10, 437–449, https://doi.org/10.5194/cp-10-437-2014, 2014.

Briffa, K. R., Osborn, T. J., Schweingruber, F. H., Jones, P. D., Shiyatov, S. G., and Vaganov, E. A.: Tree-ring width and density data around the Northern Hemisphere: Part 1, local and regional climate signals, Holocene, 12, 737–757, https://doi.org/10.1191/0959683602hl587rp, 2002.

Briffa, K. R., Osborn, T. J., and Schweingruber, F. H.: Large-scale temperature inferences from tree rings: a review, Glob. Planet. Change, 40, 11–26, https://doi.org/10.1016/S0921-8181(03)00095-X, 2004.

Dai, A., Trenberth, K. E., and Qian, T.: A global data set of Palmer Drought Severity Index for 1870-2002: Relationship with soil moisture and effects of surface warming, J. Hydrometeorology, 5, 1117–1130, https://doi.org/10.1175/JHM-386.1, 2004.

Gaspari, G. and Cohn, S. E.: Construction of correlation functions in two and three dimensions, Quart. J. Roy. Meteor. Soc., 125, 723–757, https://doi.org/10.1002/qj.49712555417, 1999.

PAGES 2k Consortium: A global multiproxy database for temperature reconstructions of the Common Era, Sci. Data, 4, https://doi.org/10.1038/sdata.2017.88, 2017.

Schneider, U., Becker, A., Finger, P., Meyer-Christoffer, A., Ziese, M., and Rudolf, B.: GPCC's new land surface precipitation climatology based on quality-controlled in situ data and its role in quantifying the global water cycle, Theoretical and Applied Climatology, 115, 15–40, https://doi.org/10.1007/s00704-013-0860-x, 2014.

St. George, S.: An overview of tree-ring width records across the Northern Hemisphere, Quaternary Science Reviews, 95, 132–150, https://doi.org/10.1016/j.quascirev.2014.04.029, 2014.

St. George, S., Meko, D. M., and Cook, E. R.: The seasonality of precipitation signals embedded within the North American Drought Atlas, The Holocene, 20, 983–988, https://doi.org/10.1177/0959683610365937, 2010.

Steiger, N. J., Smerdon, J. E., Cook, E. R., and Cook, B. I.: A reconstruction of global hydroclimate and dynamical variables over the Common Era, Sci. Data, 5, https://doi.org/10.1086/sdata.2018.86, 2018.

Table S1: Summary of instrumental–era verification results for reconstructions performed with various tree-ring width PSM configurations (see main text, section 2.4.2 for PSM details). Verification scores shown are correlation (r) and coefficient of efficiency (CE) for the annual global mean temperature (GMT) and detrended GMT verified against the consensus of instrumental–era analyses, the global mean of gridpoint r and CE characterizing the spatially reconstructed temperature, verified against the Berkeley Earth analysis.

PSM configuration	Annual GMT		Detrended GMT		Spatial temperature	
	r	CE	r	CE	r	CE
Univariate "TorM" (PDSI)	0.92	0.79	0.72	0.46	0.52	0.17
Univariate "TorM" (precip.)	0.93	0.77	0.74	0.48	0.53	0.17
Bivariate	0.93	0.86	0.77	0.54	0.53	0.20

Table S2: Verification of reconstructions against independent (withheld from assimilation) proxies, for experiments using various PSM configurations to model tree-ring width proxies. Skill scores shown are the median of distributions for correlation (r), the fraction of proxy records characterized by a positive ΔCE (%+CE), and the median of the ΔCE distribution. Statistics are compiled over 51 Monte-Carlo realizations, for two distinct periods: 1880–2000 (PSM calibration period) and 0–1879 (pre-calibration period).

PSM configuration	1880–2000				0–1879			
	r	%+CE	ΔCE	ECR	r	%+CE	ΔCE	ECR
Univariate "TorM" (PDSI)	0.34	80.0	0.09	0.94	0.21	70.4	0.05	1.06
Univariate "TorM" (precip.)	0.33	77.6	0.08	0.93	0.19	66.3	0.04	1.06
Bivariate	0.36	78.9	0.11	0.93	0.22	66.0	0.06	1.08

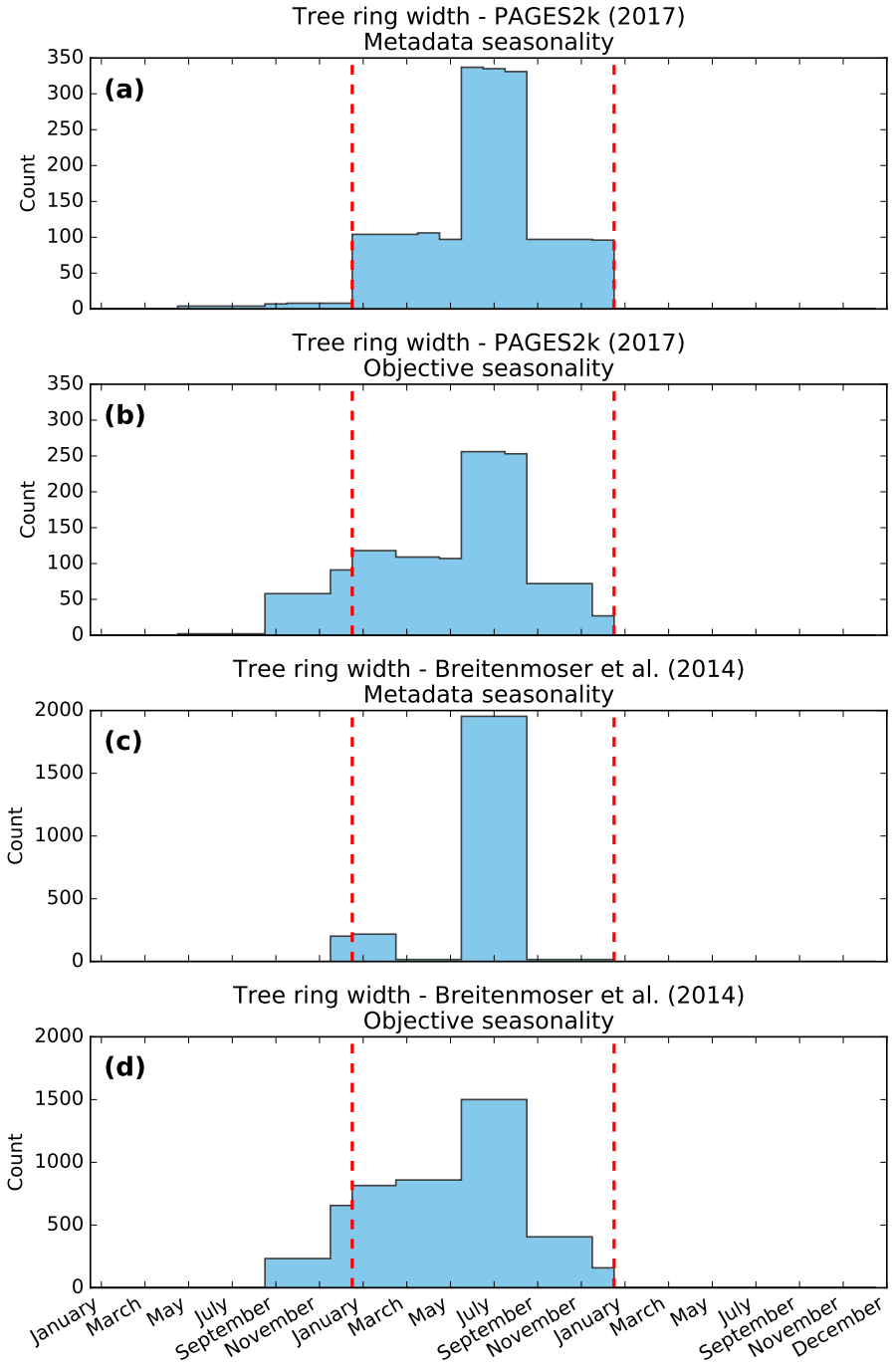

Figure S1: Distributions of months of the year included in proxy seasonal responses for tree ring records in (a) and (b) PAGES 2k Consortium (2017), (c) and (d) Breitenmoser et al. (2014) data sets. For each proxy set, histograms are shown describing the seasonality information contained in (a) and (c) the proxy metadata, and (b) and (d) objectively-derived during PSM calibration using a goodness-of-fit approach. Vertical dashed red lines delineate the annual period of the modeled proxy. PSM calibration is performed with respect to temperature, using the GISTEMP v4 dataset.

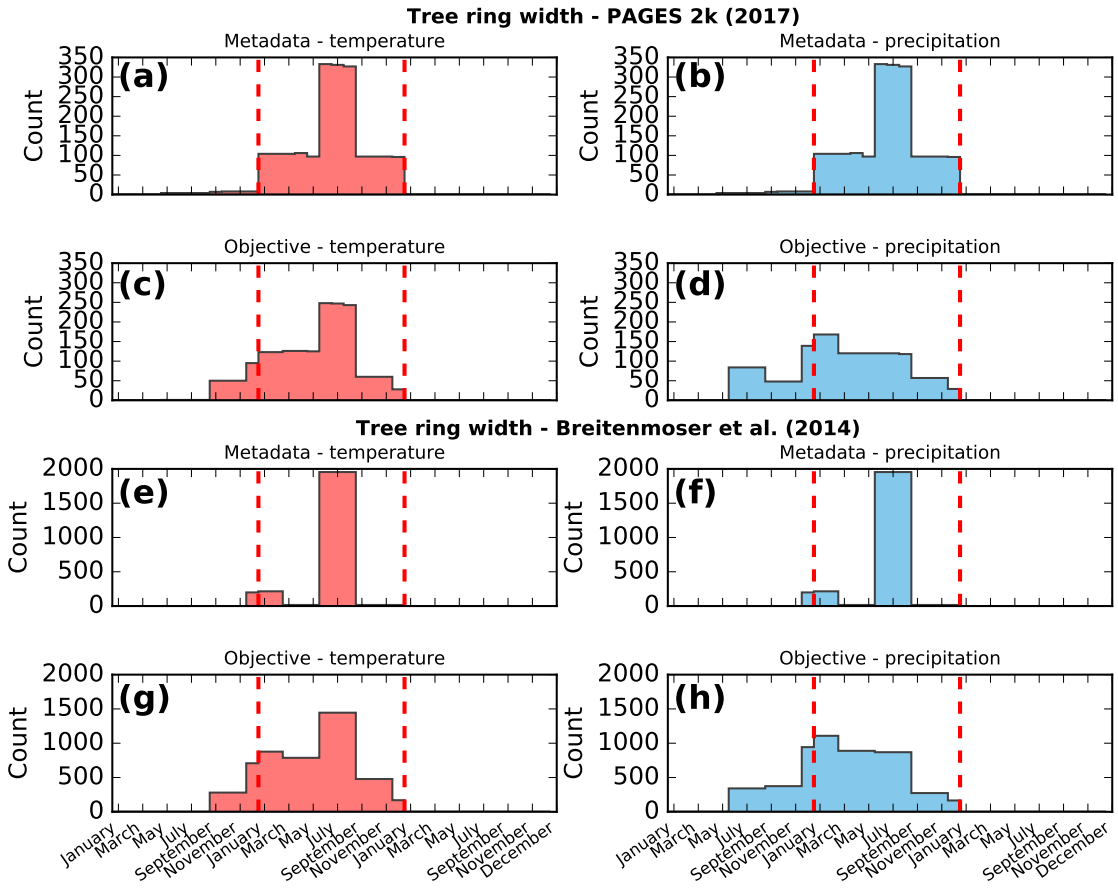

Figure S2: As in Fig. S1, but for seasonal responses of temperature and precipitation used in the bivariate TRW PSMs, for tree ring records in (a)–(d) PAGES 2k Consortium (2017), (e)–(h) Breitenmoser et al. (2014) data sets. For each proxy set, histograms are shown describing the seasonality information contained in (a), (b), (e) and (f) the proxy metadata, and (c), (d), (g) and (h) objectively-derived using a goodness-of-fit approach during PSM calibration. Distributions for temperature are shown in the left panels, and for precipitation in the right panels. Bivariate PSM calibration is performed with respect to temperature and precipitation, using the GISTEMP v4 and GPCC v6 datasets.

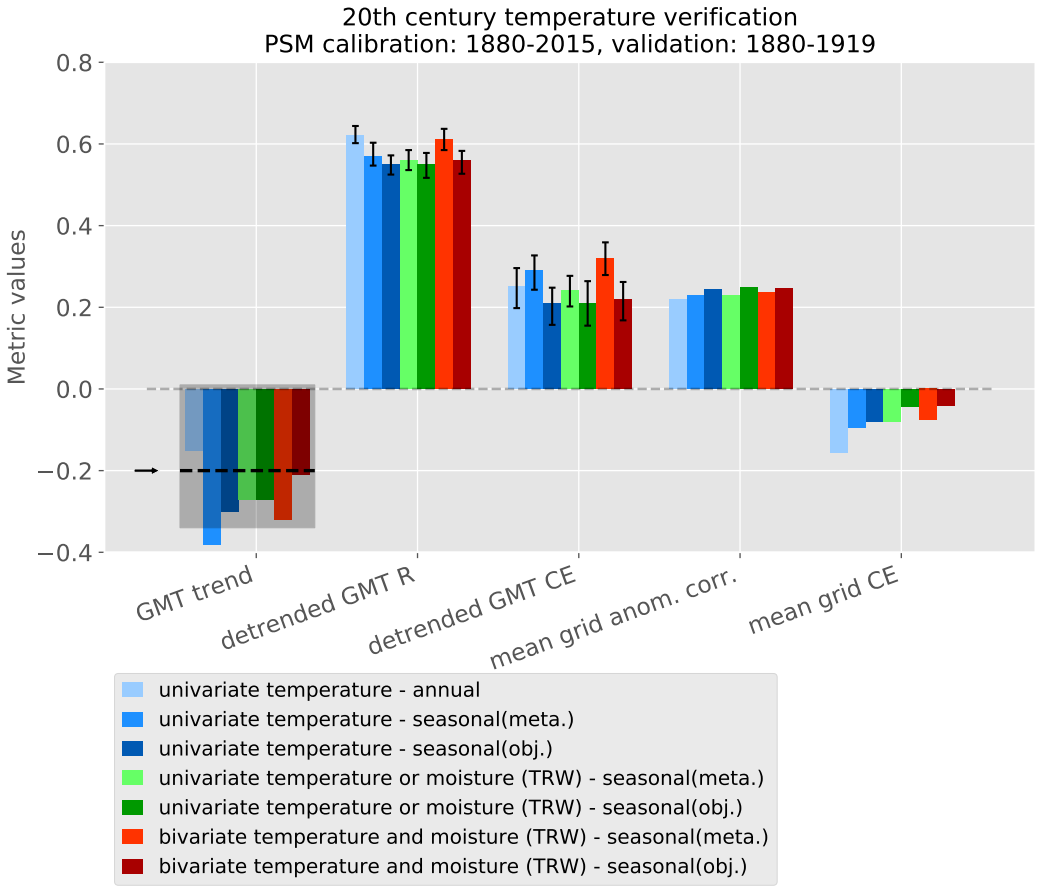

Figure S3: Summary skill metrics of LMR temperature reconstructions against the consensus of instrumental era temperature data sets (GISTEMP, MLOST, Berkeley Earth, HadCRUT4) over the 1880–1919 period. Reconstruction experiments are performed with PSMs calibrated on data covering the 1920–2015 period (excluding the verification period) with the following PSM configurations: univariate on annual temperature (light blue), univariate on seasonal (metadata) temperature (blue), univariate seasonal models with objectively-derived seasonality (dark blue), seasonal (metadata) univariate "temperature or moisture" for tree ring widths and temperature only for all other proxies (light green), same as previous but with objectively-derived seasonality (dark green), bivariate seasonal (metadata) models for tree ring widths and univariate on temperature for all other proxies (red) and same as previous but with objectively-derived seasonality (dark red). Metrics shown are the 20th century trend in the global mean temperature (GMT), correlation and coefficient of efficiency (CE) for the detrended GMT, mean of anomaly correlations against the instrumental data sets, and global mean of gridpoint CE averaged across the same verification data sets. The GMT trend from consensus of instrumental-era products is shown by the arrow and dashed black line, along with the range defined by the individual instrumental-era products shown by the gray-shaded area. Error bars are the 5-95% bootstrap confidence intervals on the corresponding skill metric.

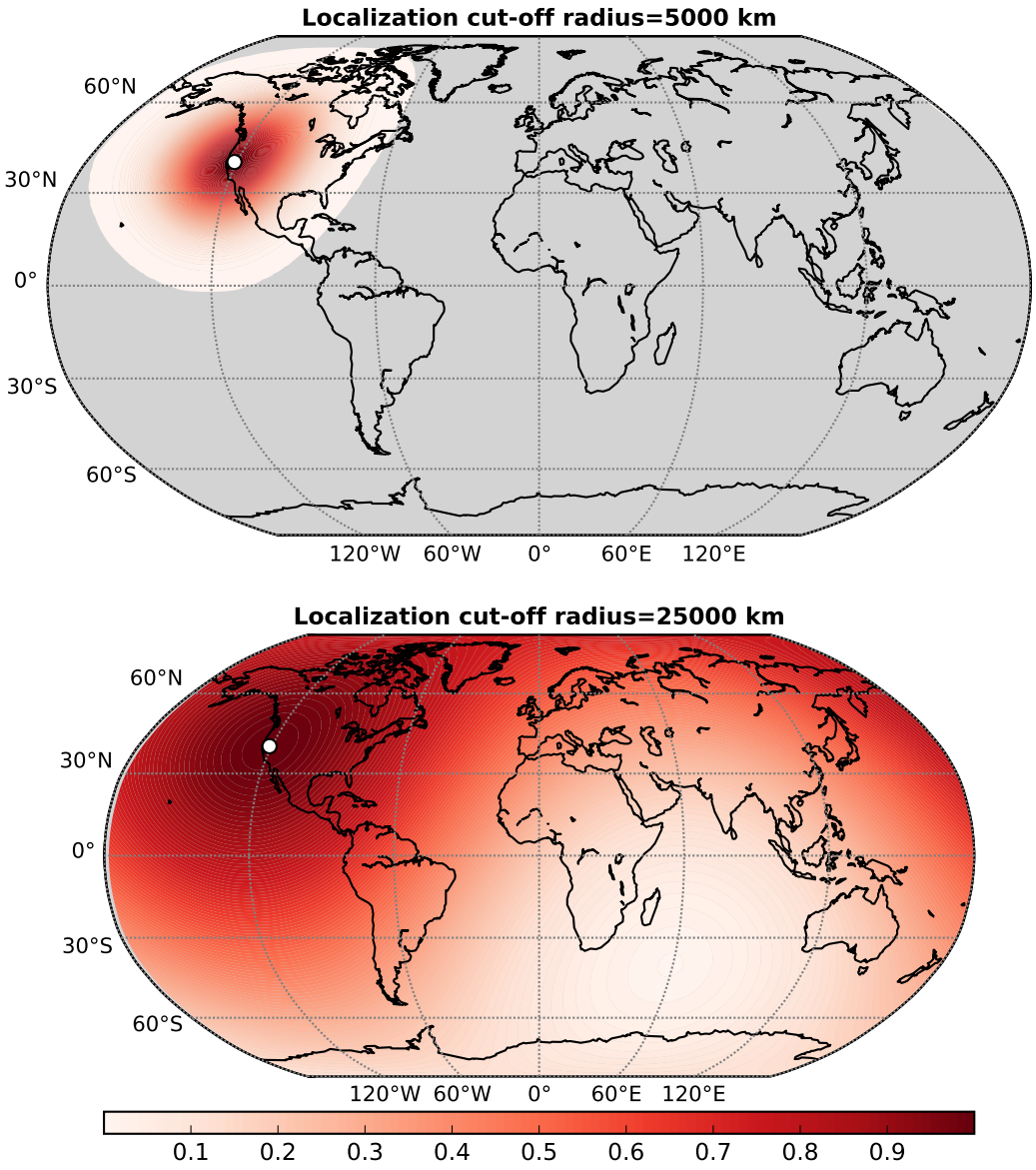

Figure S4: Gaspari-Cohn localization function (w_{loc} in Eqs. 4 in the main text) corresponding to a proxy site located in the Sierra Nevada mountains in California, calculated using two cut-off distances: 5000 km (upper frame) and 25000 km (lower frame). Areas shaded in gray indicate regions where w_{loc} is zero.